Yan, Ruoyu; Wang, Weijun; Vuong, Thu V.; Xiu, Yang; Skarina, Tatiana; Di Leo, Rosa; Gatenholm, Paul; Toriz, Guillermo; Tenkanen, Maija; Stogios, Peter J.; Master, Emma R.

Structural characterization of the family GH115 α-glucuronidase from Amphibacillus xylanus yields insight into its coordinated action with α-arabinofuranosidases

Published in:
NEW BIOTECHNOLOGY

DOI:
10.1016/j.nbt.2021.01.005

Published: 25/05/2021

Document Version
Publisher's PDF, also known as Version of record

New BIOTECHNOLOGY 62 (2021) 49–56

Contents lists available at ScienceDirect

New BIOTECHNOLOGY

journal homepage: www.elsevier.com/locate/nbt

Full length Article

Structural characterization of the family GH115 α-glucuronidase from *Amphibacillus xylanus* yields insight into its coordinated action with α-arabinofuranosidases

Ruoyu Yan [a], Weijun Wang [a], Thu V. Vuong [a], Yang Xiu [a], Tatiana Skarina [a], Rosa Di Leo [a], Paul Gatenholm [b], Guillermo Toriz [c], Maija Tenkanen [d], Peter J. Stogios [a], Emma R. Master [a,e,*]

[a] Department of Chemical Engineering and Applied Chemistry, University of Toronto, 200 College Street, Toronto, Ontario, M5S 3E5, Canada
[b] Department of Chemistry and Chemical Engineering, Wallenberg Wood Science Center and Biopolymer Technology, Chalmers University of Technology, Kemivägen 4, Gothenburg, 412 96, Sweden
[c] Department of Wood, Cellulose and Paper Research, University of Guadalajara, Guadalajara, 44100, Mexico
[d] Department of Food and Environmental Sciences, University of Helsinki, P.O. Box 27, Helsinki, 00014, Finland
[e] Department of Bioproducts and Biosystems, Aalto University, FI-00076, Aalto, Kemistintie 1, Espoo, Finland

ARTICLE INFO

Keywords:
α-Arabinofuranosidase
α-Glucuronidase
Arabinoglucuronoxylan
Hemicellulases
GH115
GH51
GH62

ABSTRACT

The coordinated action of carbohydrate-active enzymes has mainly been evaluated for the purpose of complete saccharification of plant biomass (lignocellulose) to sugars. By contrast, the coordinated action of accessory hemicellulases on xylan debranching and recovery is less well characterized. Here, the activity of two family GH115 α-glucuronidases (SdeAgu115A from *Saccharophagus degradans*, and AxyAgu115A from *Amphibacillus xylanus*) on spruce arabinoglucuronoxylan (AGX) was evaluated in combination with an α-arabinofuranosidase from families GH51 (AniAbf51A, aka E-AFASE from *Aspergillus niger*) and GH62 (SthAbf62A from *Streptomyces thermoviolaceus*). The α-arabinofuranosidases boosted (methyl)-glucuronic acid release by SdeAgu115A by approximately 50 % and 30 %, respectively. The impact of the α-arabinofuranosidases on AxyAgu115A activity was comparatively low, motivating its structural characterization. The crystal structure of AxyAgu115A revealed increased length and flexibility of the active site loop compared to SdeAgu115A. This structural difference could explain the ability of AxyAgu115A to accommodate more highly substituted arabinoglucuronoxylan, and inform enzyme selections for improved AGX recovery and use.

Introduction

Xylans from coniferous wood and agricultural fibre comprise a β-(1→4)-linked D-xylopyranosyl (Xyl*p*) backbone, partially substituted at O-2 positions with 4-*O*-(methyl)glucopyranosyluronic acid (MeGlc*p*A) and at O-3 positions with arabinofuranosyl (Ara*f*) residues [1,2]. These xylans differ in relative abundance of Ara*f* and MeGlc*p*A substituents, where arabinoglucuronoxylan from conifers typically contain higher levels of MeGlc*p*A than Ara*f*; the reverse is generally the case for glucuronoarabinoxylans from agricultural fibre. Accordingly, the complete biological conversion of xylans to monosaccharides requires the action of multiple main-chain and side-group cleaving enzymes [3]. To date, the coordinated action of corresponding enzymes has been studied mainly to generate fermentable sugars used to produce biofuels and commodity chemicals [4–6]. Alternatively, accessory enzymes alone could be used to recover and tailor high molecular weight xylans for application in food and bio-based materials [7–13].

Examples of accessory hemicellulases relevant to xylan processing include α-arabinofuranosidases (3.2.1.55) and α-glucuronidases (3.2.1.131) that target side-group residues of arabinoglucuronoxylan (Fig. 1). Xylan-active α-arabinofuranosidases (i.e., arabinoxylan arabinofuranohydrolases; AXH) reported to date release α-(1→3)-L-Ara*f*

Abbreviations: ABF, α-arabinofuranosidase; AniAbf51A, a GH51 α-arabinofuranosidase from *Aspergillus niger* (aka E-AFASE); AGX, arabinoglucuronoxylan; AXH, arabinoxylan arabinofuranohydrolase; AxyAgu115A, a GH115 α-glucuronidase from *Amphibacillus xylanus*; GH, glycoside hydrolase; SdeAgu115A, a GH115 α-glucuronidase from *Saccharophagus degradans*; SthAbf62A, a GH62 α-arabinofuranosidase from *Streptomyces thermoviolaceus*.

* Corresponding author at: Department of Chemical Engineering and Applied Chemistry, University of Toronto, 200 College Street, Toronto, Ontario, M5S 3E5, Canada.
E-mail address: emma.master@utoronto.ca (E.R. Master).

https://doi.org/10.1016/j.nbt.2021.01.005
Received 24 June 2020; Received in revised form 11 January 2021; Accepted 16 January 2021
Available online 21 January 2021

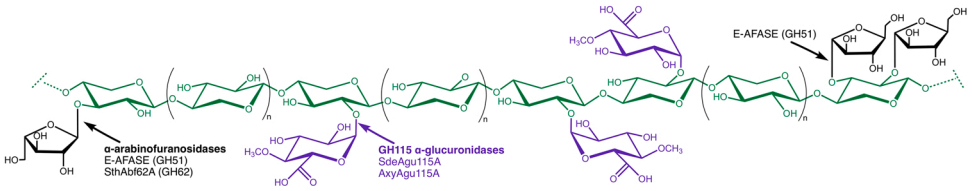

Fig. 1. Both α-arabinofuranosidases and α-glucuronidases are required to remove substituents from spruce arabinoglucuronoxylan. The number of D-xylopyranosyl unit, n, is generally from 1 to 6 [36].

substituents from di-substituted Xyl*p* subunits along the xylan backbone (i.e., AXH-d3 activity), or release α-(1→3)-L-Ara*f* and α-(1→2)-L-Ara*f* from mono-substituted Xyl*p* (i.e., AXH-m 2,3 activity). Whereas certain enzymes belonging to glycoside hydrolase (GH) family GH43 display AXH-d3 activity, AXH-m 2,3 activity is displayed by arabinoxylan arabinofuranohydrolases belonging to families GH43 and GH62 [14–21]. For example, our earlier study of the family GH62 α-arabinofuranosidase, StAbf62A from *Streptomyces thermoviolaceus*, confirmed its selective action towards L-Ara*f* residues that are α-(1→2) and α-(1→3) linked to mono-substituted D-Xyl*p* of wheat arabinoxylan [21]. Studies by other groups have reported GH51 and GH54 enzymes with AXH-m, d type activity towards the non-reducing end terminal Xyl*p* of oligosaccharides; however, in these cases, only weak activity is detected towards internal Ara*f* substitutions in polymeric arabinoxylans [22–25].

Xylan-active α-glucuronidases are currently classified into families GH67 and GH115. GH67 activity is restricted to MeGlc*p*A residues at the non-reducing end of the substrate; by contrast, xylan-active GH115 enzymes are able to remove MeGlc*p*A from both terminal and internal positions of the xylan backbone [26–28]. Our earlier studies of SdeAgu115A from *Saccharophagus degradans* and AxyAgu115A from *Amphibacillus xylanus* confirmed their action on a variety of xylan sources, including beechwood glucuronoxylan, spruce arabinoglucuronoxylan (AGX) and oat spelt glucuronoarabinoxylan, and also revealed the higher performance of AxyAgu115A on comparatively complex xylans [28,29]. SdeAgu115A and AxyAgu115A are 972 and 966 amino acids in length and are 32 % identical over the full lengths of their sequences. A 3-D model of AxyAgu115A based on the X-ray structure of SdeAgu115A predicted flexible loop regions within the AxyAgu115A active site that could play a role in its accommodation of complex xylans [29].

To delve deeper into structure-function relationships of family GH115 xylan-active α-glucuronidases, the potential of selected α-arabinofuranosidases to boost the performance of AxyAgu115A and SdeAgu115A action towards spruce arabinoglucuronoxylan was investigated. The X-ray structure of AxyAgu115A was also solved, which confirms the increased length and flexibility of the active-site loop in AxyAgu115A compared to SdeAgu115A, potentially explaining the ability of AxyAgu115A to accommodate more highly substituted arabinoglucuronoxylan.

Materials and methods

Materials

Spruce arabinoglucuronoxylans (AGX) were isolated from a debarked spruce log (*Picea abies*), provided by the Wallenberg Wood Science Center (Stockholm, Sweden), based on a previously reported method [10], and were further purified by bleaching with hydrogen peroxide. Briefly, AGX (1 g) was dissolved in deionized water, pentetic acid (Sigma-Aldrich, St. Louis, MO, USA) was added (1.2 wt. % relative to the weight of xylan) to complex ions, and then left stirring overnight. Sodium silicate (Sigma-Aldrich) was then added (2.25 wt %), and the temperature was raised to 50 °C before adding hydrogen peroxide (600 μL; 50 %) (Sigma-Aldrich) and adjusting the pH to pH 11.0. After 4 h, the AGX was precipitated in acidic ethanol (4:1, v/v of ethanol to xylan), prepared with ethanol 96 % (Sigma-Aldrich) and glacial acetic acid (Sigma-Aldrich) (1:0.1, v/v). The solution was then dialyzed against deionized water for 3 d using a 1 kDa molecular weight cut-off dialysis membrane (Thermo Fisher Scientific, Waltham, MA, USA). GH51 α-L-arabinofuranosidase (AniAbf51A, aka E-AFASE from *Aspergillus niger*), as well as the D-glucuronic acid assay kit and L-arabinose assay kit, were from Megazyme (Bray, Ireland). Buffer exchange was performed using Amicon Ultra 0.5 mL centrifugal filters with molecular weight cut-off at 10 kDa (Millipore, Oakville, ON, Canada). SdeAgu115A from *Saccharophagus degradans 2-40T* [28], AxyAgu115A from *Amphibacillus xylanus* [29], and SthAbf62A from *Streptomyces thermoviolaceus* [21] were produced in our laboratory based on previously published methods.

Coordinated action of α-glucuronidases and α-arabinofuranosidases on AGX

Based on the general biochemical properties of the selected enzymes (Table 1), the standard reaction was performed at 40 °C for 20 min in 67

Table 1
General properties of the accessory xylan-acting enzymes selected for this study.

[a]Enzyme	GH family	Optimal pH	Optimal temperature	Enzyme specificity	Substrate (assay condition)	Specific activity (μmol product/min/mg protein)	References
SdeAgu115A	115	6.5	40 °C	Remove α-(1→2)-MeGlc*p*A substituents	Spruce arabinoglucuronoxylan (1.0 %, w/v, pH 6.5)	8.3 ± 0.1	Wang et al. [28]
AxyAgu115A	115	7.0	55 °C	Remove α-(1→2)- MeGlc*p*A substituents	Spruce arabinoglucuronoxylan (1.0 %, w/v, pH 7.0)	51.2 ± 0.6	Yan et al. [29]
SthAbf62A	62	7.0	55 °C	Remove α-(1→2)-Ara*f* and α-(1→3)-Ara*f* mono-substituents	Wheat arabinoxylan (0.5 %, w/v, pH 6.5)	40 ± 3	Wang et al. [21]
AniAbf51A	51	4.0	50 °C	Remove α-(1→2)-Ara*f* and α-(1→3)-Ara*f* mono-substituents and Ara*f* disubstitutions	Wheat arabinoxylan (1.0 %, w/v, pH 4.0)	1.2	McCleary et al. [24]

[a] All enzymes remained active at selected universal assay condition for synergistic study, namely 40 °C at pH 7.0.

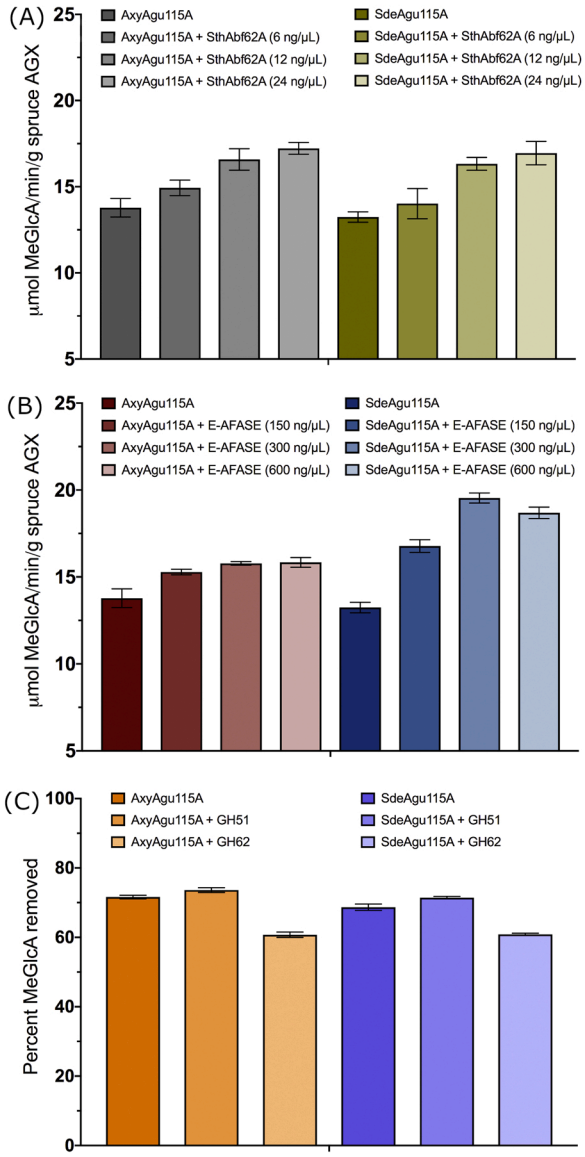

Fig. 2. Rate and extent of MeGlc*p*A released from arabinoglucuronoxylan (AGX) by the concerted action of selected α-glucuronidases and α-arabinofuranosidases. MeGlc*p*A release rates by two α-glucuronidases, AxyAgu115A (9 ng/µL) and SdeAgu115A (40 ng/µL), with increasing amounts of SthAbf62A (6, 12 and 24 ng/µL) (A), or with increasing amounts of AniAbf51A (150, 300, and 600 ng/µL) (B). To determine rates of MeGlc*p*A release, reactions were performed for 20 min at 40 °C in 67 mM universal buffer at pH 7.0 using 1 % (w/v) AGX. The doses of SthAbf62A and AniAbf51A were adjusted to obtain similar levels of α-arabinofuranosidase activity. The percent of MeGlc*p*A released from AGX after 24 h in the absence and presence of 0.6 µg/µL SthAbf62A or AniAbf51A (C). Error bars represent standard deviation; n = 3.

mM universal buffer (0.067 M H_3BO_3, 0.067 M H_3PO_4, 0.067 M CH_3COOH, adjusted to pH 7.0 using a sodium hydroxide solution); each individual enzyme was validated under this condition (Suppl. Figure S1). Final concentrations of AxyAgu115A and SdeAgu115A in corresponding reaction mixtures were optimized to obtain initial rates of reaction, and were 9 ng/µL and 40 ng/µL, respectively. Three doses of SthAbf62A or AniAbf51A were used to supplement GH115 activity, where enzyme loadings were adjusted to achieve similar activity levels. Accordingly, the three SthAbf62A doses were 6 ng/µL, 12 ng/µL and 24 ng/µL, whereas the three AniAbf51A doses were 150 ng/µL, 300 ng/µL and 600 ng/µL. After 20 min, reactions were heated to 100 °C for 10 min to inactivate the enzyme activity. A typical enzymatic reaction mixture contained 10 µL of enzyme cocktail and 20 µL of 1 % (w/v) spruce AGX, representing a final substrate concentration at 0.67 % (w/v). The released MeGlc*p*A and Ara*f* were quantified by D-glucuronic acid assay kit and L-arabinose assay kit, respectively.

To evaluate the impact of α-arabinofuranosidases on the extent of MeGlc*p*A released by AxyAgu115A and SdeAgu115A, reaction mixtures were prepared as described above and contained 0.6 µg/µL GH115 α-glucuronidase (SdeAgu115A or AxyAgu115A) and 0.6 µg/µL α-arabinofuranosidase (AniAbf51A or SthAbf62A). Following 24 h of incubation at 25 °C, MeGlc*p*A and Ara*f* released were quantified using a D-glucuronic acid assay kit and L-arabinose assay kit, respectively.

Protein crystallization, data collection, and structure determination

The *E. coli* codon-optimized *axyggu115A* gene (locus tag AXY_23000 from *Amphibacillus xylanus* NBRC 15112) (Suppl. Figure S2) was purchased from Genscript (Piscataway, NJ, USA) and subcloned into the p15-Tv-LIC vector (The Structural Genomics Consortium, Toronto, ON, Canada), coding for a fusion protein with N-terminal His_6-tag and TEV protease cleavage site. As this improved crystal quality according to the surface entropy reduction approach and the SerP server [30], the triple mutant K79A, K80A and E81A of AxyAgu115A enzyme was cloned using a Quikchange mutagenesis kit (Agilent Technologies, Santa Clara, CA, USA). The AxyAgu115A enzyme was purified as previously described

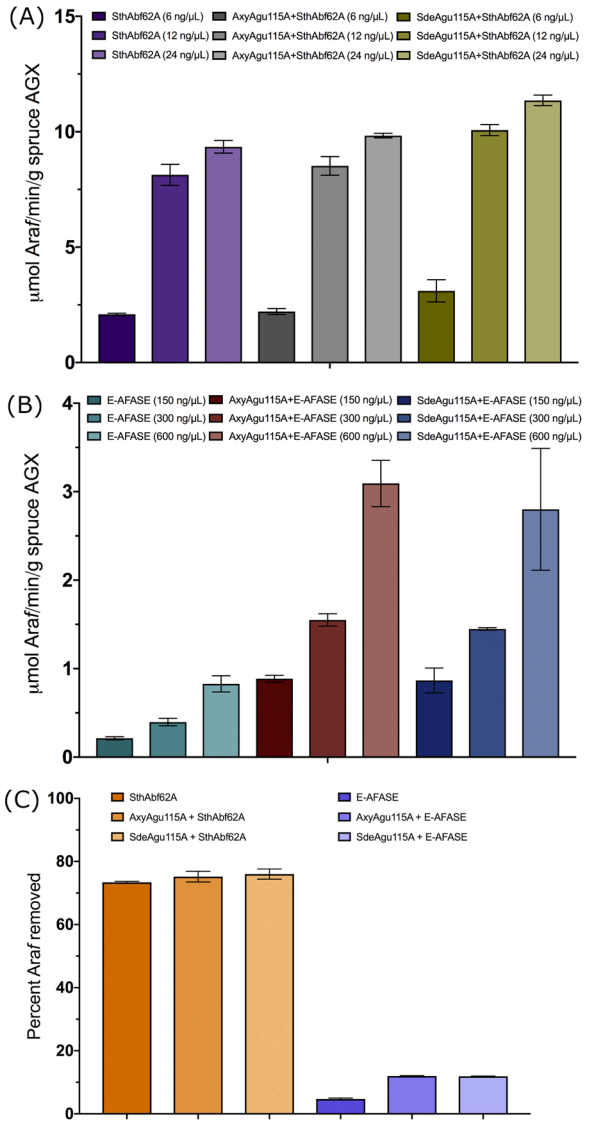

Fig. 3. Rate and extent of Ara*f* released from arabinoglucuronoxylan (AGX) by the concerted action of selected α-glucuronidases and α-arabinofuranosidases. Ara*f* release rates by SthAbf62A (6, 12 and 24 ng/μL) (A) or by AniAbf51A (150, 300, and 600 ng/μL) (B) in the presence of AxyAgu115A (9 ng/μL) or SdeAgu115A (40 ng/μL). (C) The percent of Ara*f* released from AGX after 24 h in the absence and presence of 0.6 μg/μL AxyAgu115A or SdeAgu115A. Error bars represent standard deviation; n = 3.

[29]. Crystals of AxyAgu115A^{K79AK80AE81A} were grown using the sitting-drop method with 0.5 μL of 20 mg/mL protein solution with 0.5 μL of reservoir solution 20 % (w/v) PEG 3350, 0.2 M diammonium hydrogen citrate and 10 mM D-glucuronic acid (Sigma-Aldrich, St. Louis, MO, USA). Crystals were cryoprotected in paratone oil (Hampton Research, Aliso Viejo, CA, USA) before flash-freezing in liquid nitrogen. X-ray diffraction data was collected at 100 K at beamline 21-ID-D at the Life Sciences Collaborative Access Team, Advanced Photon Source, Argonne National Laboratory (Lemont, IL, USA). Diffraction data was processed by XDS [31] and Aimless [32]. The structure was solved by Molecular Replacement with Phenix.phaser [33] using models of AxyAgu115A generated by the Phyre2 server [34] and the three N-terminal domains of SdeAgu115A [28] and BoAgu115A [27]. Automated model building from the initial MR solution was performed using Phenix.autobuild. Manual model building and refinement were performed using Coot [35] and Phenix.refine with TLS parameterization, and all B-factors were refined as isotropic. Electron density in the active site was modeled as glycerol molecules. Structure figures were prepared using PyMol (Schrödinger LLC, New York, NY, USA).

Docking analysis

The PDB IDs of SdeAgu115A and SthAraf62A are 4ZMH and 4O8N, respectively, while the X-ray structure of AxyAgu115A was solved in this study (PDB ID: 6NPS). The dimeric structures of SdeAgu115A and AxyAgu115A were used for computational docking. The structural model of AniAbf51A was built based on a *Thermobacillus xylanilyticus* GH51 arabinofuranosidase (PDB ID: 2VRQ) by the Phyre2 server [34]. Based on the mass spectrometry MS/MS analysis of spruce AGX [36], three xylohexaoses with a different substitution pattern were used: (1) one MeGlc*p*A α-(1→2)-linked to Xyl*p* in the -2 position (XXXXU^{4m2}X), (2) an MeGlc*p*A α-(1→2)-linked to Xyl*p* in the -2 position and an Ara*f* α-(1→3)-linked to a Xyl*p* in the -4 position (XXA$_3$XU^{4m2}X); and (3) two MeGlc*p*A substituents α-(1→2)-linked to consecutive Xyl*p* residues in the -2 and -3 positions (XXXU^{4m2}U^{4m2}X). The 3D structures of these oligosaccharide ligands were drawn by ChemBioDraw v11.0.2 (PerkinElmer, Waltham, MA, USA).

AutodockTools v1.5.2 on Python v2.5 (http://autodock.scripps.edu) was then used to prepare the proteins and ligands, and to setup grid boxes. Docking simulation was conducted using Autodock Vina v1.1.2

using default parameters (http://vina.scripps.edu). Figures were generated by PyMol (Schrödinger LLC).

Results and discussion

Comparison of AxyAgu115A and SdeAgu115A activity on spruce arabinoglucuronoxylan in the presence of selected α-arabinofuranosidases

It has been shown previously that in spruce arabinoglucuronoxylans (AGX), Ara*f* and MeGlc*p*A are evenly spaced and closely positioned, and that two MeGlc*p*A can occupy adjacent positions along the xylan backbone [36]. This close proximity of Ara*f* and MeGlc*p*A residues could impact α-glucuronidase and arabinofuranosidase activities on AGX (Fig. 1).

To investigate potential differences in AxyAgu115A and SdeAgu115A action on complex xylans like AGX, corresponding enzyme activities were measured using spruce AGX in the presence or absence of α-arabinofuranosidases, specifically AniAbf51A from family GH51 and SthAbf62A from family GH62 (Table 1). As mentioned above, AniAbf51A displays dual ABF-m/d activity, and targets α-(1→2)-Ara*f* and α-(1→3)-Ara*f* mono-substituents, as well as Ara*f* disubstitutions of non-reducing end Xyl*p* residues [23; 24]. By contrast, SthAbf62A acts on L-Ara*f* residues that are α-(1→2) and α-(1→3) linked to mono-substituted D-Xyl*p* [21].

SthAbf62A increased the activity of both AxyAgu115A and SdeAgu115A by up to 28 % in a dose-dependent manner (Fig. 2A). On the other hand, the extent of MeGlc*p*A released from AGX after 24 h by the α-glucuronidases decreased by approximately 15 % in reactions containing SthAbf62A (Fig. 2C). Although small, this reproducible impact on MeGlc*p*A release by both α-glucuronidases showed that steric hindrance caused by Ara*f* can be quickly alleviated with addition of SthAbf62A, but that once this constraint is overcome, reduced substrate solubility resulting from Ara*f* removal from AGX can hinder α-glucuronidase performance [37,38].

In contrast to SthAbf62A, the impact of AniAbf51A on α-glucuronidase activity was enzyme dependent, where AniAbf51A increased SdeAgu115A activity by 48 %, but only by 15 % for AxyAgu115A (Fig. 2B). AniAbf51A is distinguished from SthAbf62A by its ability to target Ara*f* disubstitutions [24]. The lower impact of AniAbf51A on AxyAgu115A compared to SdeAgu115A, therefore, suggests that AxyAgu115A activity is less hindered by nearby di-substitutions of the xylan backbone [29].

SthAbf62A activity and performance was not significantly impacted by the presence of AxyAgu115A or SdeAgu115A (Fig. 3A, C). Conversely, rates of Ara*f* release by AniAbf51A increased by approximately 300 % in the presence of either α-glucuronidase (Fig. 3B); the extent of Ara*f* released by AniAbf51A also increased by more than 200 % in reactions supplemented with either α-glucuronidase (Fig. 3C).

To investigate further the structural basis for the lower impact of AniAbf51A on AxyAgu115A activity and performance, the crystal structure of AxyAgu115A was solved to permit direct comparations with the previously reported structure for SdeAgu115A [28].

AxyAgu115A adopts a 5-domain dimeric structure, similar to SdeAgu115A

Since efforts to crystalize the wild-type enzyme were unsuccessful, a triple mutant of AxyAgu115A, AxyAgu115A^{K79AK80AE81A}, designed using the surface entropy reduction approach, was crystallized [30]. These mutations were not expected to affect enzyme activity, being on the surface and distant from the active site (Suppl. Figure S3); we therefore use the name of the wild-type enzyme, AxyAgu115A, when referring to the corresponding structure. The structure was solved by molecular replacement using the structure of SdeAgu115A [28]. All crystallographic data and refinement statistics are summarized in Table 2.

Table 2
X-ray diffraction data collection and refinement statistics.

	AxyAgu115A^{K79AK80AE81A}
PDB code	6NPS
Data collection	
Space group	P 1
Unit cell	
a, *b*, *c* (Å)	63.08, 96.21, 111.75
α, β, γ, (°)	84.37, 78.37, 83.32
Resolution, Åc	47.64 – 1.99
R_{merge} [a]	0.102 (0.534) [c]
R_{pim} [b]	0.042 (0.534)
$CC_{1/2}$	0.820
I / σ(I)	14.1 (2.2)
Completeness, %	94.6 (90.8)
Redundancy	11.9 (3.9)
Refinement	
Resolution, Å	47.64 – 1.99
No. unique reflections: working, test	165435, 8156
R-factor/free *R*-factor [d]	15.0/19.0 (24.5/26.6)
No. refined atoms, molecules	
Protein	15552, 2
Solvent	123
Water	1878
B-factors	
Protein	45.1
Solvent	86.2
Water	55.8
r.m.s.d.	
Bond lengths, Å	0.012
Bond angles, °	1.133

[a] $R_{merge} = \Sigma_{hkl}\Sigma j|I_{hkl,j} - \langle I_{hkl}\rangle|/\Sigma_{hkl}\Sigma jI_{hk,j}$, where $I_{hkl,j}$ and $\langle I_{hkl}\rangle$ are the *j*th and mean measurement of the intensity of reflection j.

[b] $R_{pim} = \Sigma_{hkl}\sqrt{(n/n\text{-}1)}\ \Sigma^{n}j=1|I_{hkl,j} - \langle I_{hkl}\rangle|/\Sigma_{hkl}\Sigma jI_{hk,j}$.

[c] all values in brackets refer to the highest resolution shell.

[d] $R = \Sigma||F_p^{obs} - F_p^{calc}|/\Sigma F_p^{obs}$, where F_p^{obs} and F_p^{calc} are the observed and calculated structure factor amplitudes, respectively.

The AxyAgu115A crystal contained two chains in its asymmetric unit, each possessing the five-domain architecture originally observed in SdeAgu115A [28] (domains A: residues 1–165, B: residues 166–477, C: residues 478–656, C+: residues 657–775 and D: residues 776–966, Fig. 4A and Suppl. Fig. S2A); the pairwise RMSD is 2.8 Å across all five domains of each of the two enzymes. The two AxyAgu115A chains in the asymmetric unit were related by non-crystallographic symmetry and interacted along an interface that buried 1,460 Å^2. This extent of buried surface as well as the fact that the packing arrangement of the two chains closely resembled that of the dimeric SdeAgu115A enzyme [28] are consistent with AxyAgu115A forming a dimer in solution (Suppl. Fig. S4B) [29]. Moreover, the arrangement of the AxyAgu115A domains involved in the dimeric interface were the same as previously observed for SdeAgu115A [28] (Fig. 4A).

The AxyAgu115A catalytic center is covered by a comparatively long and flexible loop

Similar to other GH115 crystal structures, the active site of AxyAgu115A was localized to the central cavity of domain B, a $(\beta/\alpha)_8$ TIM barrel fold (Fig. 4B and Suppl. Fig. S4C) (pairwise RMSD values with SdeAgu115A, BtGH115A and BoAgu115A are 1.3–1.5 Å, across 288–292 matching Cα atoms of domain B) [39,27,28]. Amino acids making up this putative active site were mainly found on loops of domain B; moreover, the presumed catalytic center was covered by a prominent loop from domain B (residues 301–313) (Fig. 4B). The electron density for this loop was interpretable only for one chain in the dimer (shown in Fig. 4B) while the second was more disordered and accordingly not all residues could be fully modeled. In the resolved loop, Asp305 was 4.3 Å from a trapped glycerol molecule; this residue also formed an

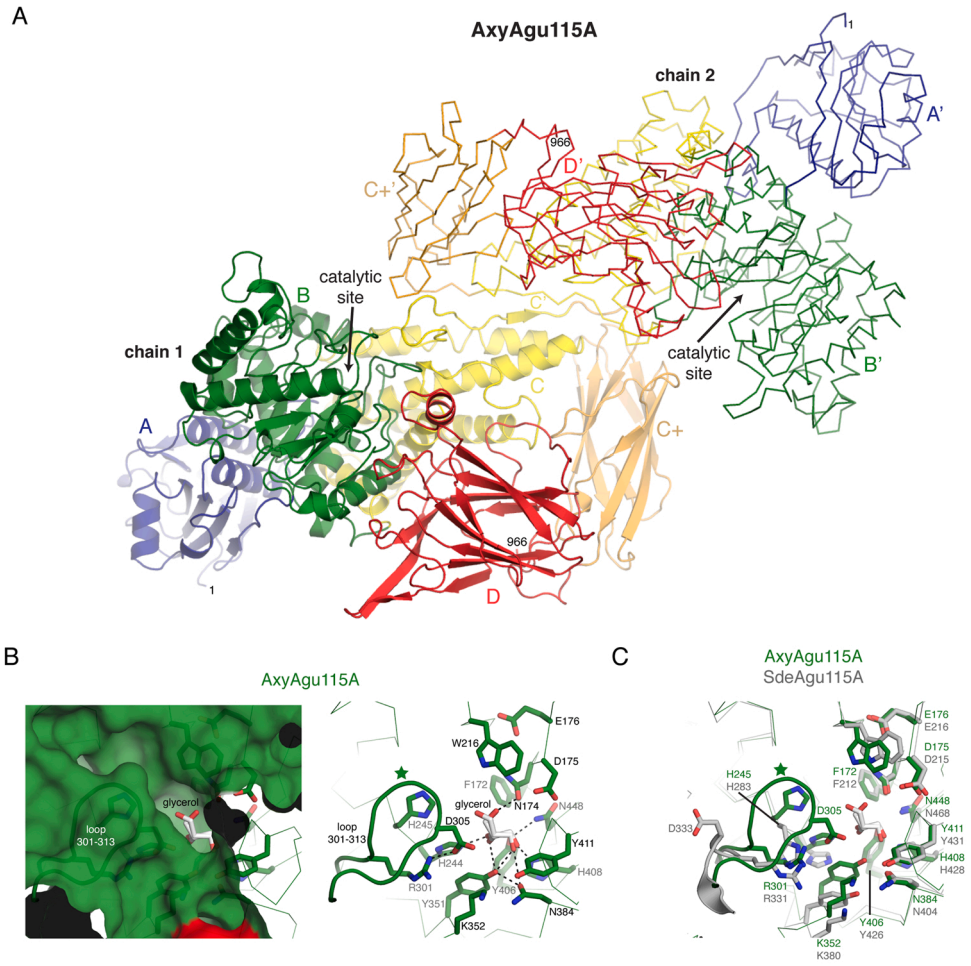

Fig. 4. Crystal structure of AxyAgu115A. (A) Overall structure of dimeric AxyAgu115A with each of the 5 domains coloured separately and labelled A, B, C, C + and D and with apostrophes for the partner subunit. The two catalytic sites are shown with arrows. Both catalytic sites are formed primarily by domain B/B' with contributions from C+'/C + . (B) Catalytic center of AxyAgu115A with enzyme shown in solvent accessible surface representation (left) and without surface (right). Glycerol bound in the catalytic center is shown as grey sticks and the loop 301-313 that forms a cap over the active site is labeled. Dashes indicate hydrogen or electrostatic interactions between active site residues or with the bound glycerol molecule. (C) Comparison of catalytic centers of AxyAgu115A (green) and SdeAgu115A (grey).

electrostatic interaction with Arg301. Notably, mutation of the residues equivalent to Arg301 in SdeAgu115A (Arg331) and BoAgu115A (Arg328) were both shown to seriously impact catalysis by those enzymes [27,28]. Beyond the conservation of this arginine residue, however, the corresponding loop differs dramatically between structurally characterized GH115 enzymes. For instance, this loop in AxyAgu115A is notably longer than for SdeAgu115A (13 residues versus 8), which is consistent with the previous structural model of AxyAgu115A [29]. Secondly, the position of Asp305 in AxyAgu115A is not structurally conserved in SdeAgu115A, and the position of Asp335 from SdeAgu115A, which was shown to be essential for catalysis, is not structurally conserved in AxyAgu115A. Thirdly, there is considerable sequence diversity in this loop region across GH115 enzymes (Suppl. Fig. S5). Collectively, these observations imply that the flexibility and sequence composition of this loop is important for recognition of substrates and determination of substrate specificity across the GH115 family.

Starting from this localization of the presumed catalytic center, the putative glucuronoxylan binding surface of AxyAgu115A was traced. As was observed for SdeAgu115A, domain C + from the partner chain in the AxyAgu115A dimer contributed to sharing the broader active site cleft (Fig. 4C, Suppl. Fig. S4C). Notably, Trp680 from the partner subunit of the dimer pointed directly into the presumed glucuronoxylan binding site. Trp177 and Trp216 from domain B and Trp643 from domain C were also prominently displayed near the catalytic center. Furthermore, electron density features near Trp177, Trp643, Trp680, His642 and His681 were modeled as four glycerol molecules (Suppl. Fig. S4C). Interestingly, these residues from domains C (His642, Trp643) and C+ (Trp680, and His681) colocalize to residues in SdeAxy115A that were shown to play a role in substrate binding (W773, W689, and F696) [28].

Binding of xylo-oligosaccharides from spruce AGX [36] to AxyAgu115, as well as SdeAgu115A, was subsequently investigated using computational docking (Fig. 5). Among three substituted xylohexaoses: $XXXXU^{4m2}X$, $XXA_3XU^{4m2}X$, and $XXXU^{4m2}U^{4m2}X$, AxyAgu115A showed the most negative docking energy to $XXXU^{4m2}U^{4m2}X$ (Fig. 5A, B, C), indicating particularly favorable interactions between AxyAgu115A and MeGlc*p*A subunits that are consecutively attached to neighboring Xyl*p* residues. Three additional H-bonds to the second MeGlc*p*A unit were revealed by docking (Suppl. Figure S6). By contrast, SdeAgu115A was predicted to interact most favorably with $XXXXU^{4m2}X$ (Fig. 5D, E, F). Interestingly, the binding modes of all ligands were flipped 180° between AxyAgu115A and SdeAgu115A (Fig. 5), likely due to the presence of the distinct long loop in AxyAgu115A, which is

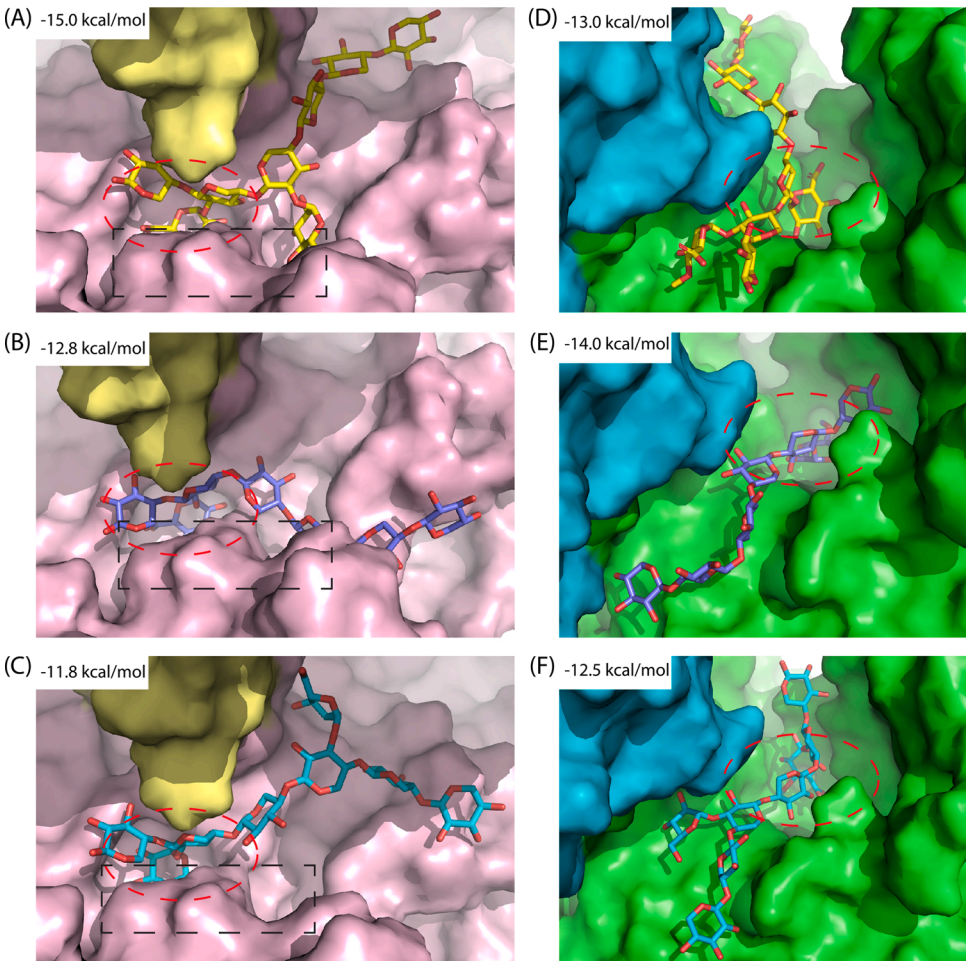

Fig. 5. Docking analysis of $XXXU^{4m2}U^{4m2}X$, $XXXXU^{4m2}X$, and $XXA_3XU^{4m2}X$ to GH115 α-glucuronidases. $XXXU^{4m2}U^{4m2}X$, $XXXXU^{4m2}X$, and $XXA_3XU^{4m2}X$ were computationally docked to AxyAgu115A X-ray structure (A, B, and C, respectively) and to SdeAgu115A X-ray structure (D, E, and F, respectively). Docking energy (kcal/mol) required for each ligand binding was shown at the top left corner of each panel. The active site of each enzyme and the distinct loop of AxyAgu115A were highlighted by red dash eclipses and black dash rectangles, correspondingly. The monomers of AxyAgu115A and SdeAgu115A dimers were differently colored: yellow - pink, and cyan - green, correspondingly.

located at the center of the active site (Fig. 5), separating two MeGlc*p*A units (Suppl. Fig. S6). Notably, SthAbf62A was predicted to bind $XXA_3XU^{4m2}X$ better than AniAbf51A (Suppl. Figure S7), which is in agreement with the lower impact of α-glucuronidases on SthAbf62A performance (Fig. 3A, C).

Conclusions

The current study has investigated the coordinated action of accessory hemicellulases that release Ara*f* and MeGlc*p*A substituents from spruce arabinoglucuronoxylan (AGX). In addition to uncovering enzyme combinations that can facilitate AGX recovery and use, the comparison of AxyAgu115A and SdeAgu115A action in the presence of α-arabinofuranosidases underscored the lower susceptibility of AxyAgu115A to steric hindrance compared to SdeAgu115A. The structural characterization of AxyAgu115A revealed a prominent, flexible loop in the active site that might contribute to the binding modes and recognition of xylo-oligosaccharides. The diversity in sequence and length of this loop region amongst family GH115 α-glucuronidases invites further studies to unravel the functional implications of its composition. Such efforts could inform GH115 selections to achieve distinct xylan forms and properties.

Authors' contributions

RY, WW, TVV, PJS and ERM conceived and designed research. RY, TVV, YX, TS, RDL and PJS conducted experiments. PG, GT and MT prepared materials. RY, PJS, TVV and ERM analyzed data and wrote the manuscript. All authors read and approved the manuscript.

Funding

This work was supported by the Government of Ontario for the project "Forest FAB: Applied Genomics for Functionalized Fibre and Biochemicals" [grant number ORF-RE-05-005], the Natural Sciences and Engineering Research Council of Canada for the Strategic Network Grant "Industrial Biocatalysis Network", and Genome Canada for the project "SYNBIOMICS - Functional genomics and techno-economic models for advanced biopolymer synthesis" (LSARP) [grant number 10405], and the European Research Council (ERC) Consolidator Grant to E.R.M. (BHIVE- 648925).

Declaration of Competing Interest

The authors report no declarations of interest.

Appendix A. Supplementary data

Supplementary material related to this article can be found, in the online version, at doi:https://doi.org/10.1016/j.nbt.2021.01.005.

References

[1] Appeldoorn MM, Kabel MA, Van Eylen D, Gruppen H, Schols HA. Characterization of oligomeric xylan structures from corn fiber resistant to pretreatment and simultaneous saccharification and fermentation. J Agric Food Chem 2010;58:11294–301. https://doi.org/10.1021/jf102849x.
[2] Willför S, Sundberg A, Hemming J, Holmbom B. Polysaccharides in some industrially important softwood species. Wood Sci Technol 2005;39:245–57. https://doi.org/10.1007/s00226-004-0280-2.

[3] Shallom D, Shoham Y. Microbial hemicellulases. Curr Opin Microbiol 2003;6:219–28.
[4] Bhattacharya AS, Bhattacharya A, Pletschke BI. Synergism of fungal and bacterial cellulases and hemicellulases: a novel perspective for enhanced bio-ethanol production. Biotechnol Lett 2015;37:1117–29. https://doi.org/10.1007/s10529-015-1779-3.
[5] de Vries RP, Kester HCM, Poulsen CH, Benen JAE, Visser J. Synergy between enzymes from Aspergillus involved in the degradation of plant cell wall polysaccharides. Carbohydr Res 2000;327:401–10. https://doi.org/10.1016/s0008-6215(00)00066-5.
[6] McKee LS, Sunner H, Anasontzis GE, Toriz G, Gatenholm P, Bulone V, et al. A GH115 α-glucuronidase from *Schizophyllum commune* contributes to the synergistic enzymatic deconstruction of softwood glucuronoarabinoxylan. Biotechnol Biofuels 2016:9. https://doi.org/10.1186/s13068-015-0417-6.
[7] Amorim C, Silvério SC, Gonçalves RFS, Pinheiro AC, Silva S, Coelho E, et al. Downscale fermentation for xylooligosaccharides production by recombinant *Bacillus subtilis* 3610. Carbohydr Polym 2019;205:176–83. https://doi.org/10.1016/j.carbpol.2018.09.088.
[8] Brennan L, Neyrinck AM, Possemiers S, Druart C, Van de Wiele T, De Backer F, et al. Prebiotic effects of wheat arabinoxylan related to the increase in bifidobacteria, roseburia and bacteroides/prevotella in diet-induced obese mice. PLoS One 2011:6. https://doi.org/10.1371/journal.pone.0020944.
[9] Chimphango AF, Gorgens JF, van Zyl WH. In situ enzyme aided adsorption of soluble xylan biopolymers onto cellulosic material. Carbohydr Polym 2016;143:172–8. https://doi.org/10.1016/j.carbpol.2016.02.012.
[10] Escalante A, Gonçalves A, Bodin A, Stepan A, Sandström C, Toriz G, et al. Flexible oxygen barrier films from spruce xylan. Carbohydr Polym 2012;87:2381–7. https://doi.org/10.1016/j.carbpol.2011.11.003.
[11] Gabrielii I, Gatenholm P, Glasser WG, Jain RK, Kenne L. Separation, characterization and hydrogel-formation of hemicellulose from aspen wood. Carbohydr Polym 2000;43:367–74. https://doi.org/10.1016/s0144-8617(00)00181-8.
[12] Höije A, Sternemalm E, Heikkinen S, Tenkanen M, Gatenholm P. Material properties of films from enzymatically tailored arabinoxylans. Biomacromolecules 2008;9:2042–7. https://doi.org/10.1021/bm800290m.
[13] Kuzmenko V, Hägg D, Toriz G, Gatenholm P. *In situ* forming spruce xylan-based hydrogel for cell immobilization. Carbohydr Polym 2014;102:862–8. https://doi.org/10.1016/j.carbpol.2013.10.077.
[14] Hashimoto K, Yoshida M, Hasumi K. Isolation and characterization of ccabf62a, a GH62 α-l-arabinofuranosidase, from the basidiomycete *Coprinopsis cinerea*. Biosci Biotechnol Biochem 2014;75:342–5. https://doi.org/10.1271/bbb.100434.
[15] Henrissat B, Davies G. Structural and sequence-based classification of glycoside hydrolases. Curr Opin Struct Biol 1997;7:637–44. https://doi.org/10.1016/s0959-440x(97)80072-3.
[16] Kimura I, Yoshioka N, Kimura Y, Tajima S. Cloning, sequencing and expression of an α-L-arabinofuranosidase from *Aspergillus sojae*. J Biosci Bioeng 2000;89:262–6. https://doi.org/10.1016/s1389-1723(00)88830-1.
[17] Maehara T, Fujimoto Z, Ichinose H, Michikawa M, Harazono K, Kaneko S. Crystal structure and characterization of the glycoside hydrolase family 62 α-L-arabinofuranosidase from *Streptomyces coelicolor*. J Biol Chem 2014;289:7962–72. https://doi.org/10.1074/jbc.M113.540542.
[18] Sakamoto T, Ogura A, Inui M, Tokuda S, Hosokawa S, Ihara H, et al. Identification of a GH62 α-L-arabinofuranosidase specific for arabinoxylan produced by *Penicillium chrysogenum*. Appl Microbiol Biotechnol 2010;90:137–46. https://doi.org/10.1007/s00253-010-2988-2.
[19] Siguier B, Haon M, Nahoum V, Marcellin M, Burlet-Schiltz O, Coutinho PM, et al. First structural insights into α-L-arabinofuranosidases from the two GH62 glycoside hydrolase subfamilies. J Biol Chem 2014;289:5261–73. https://doi.org/10.1074/jbc.M113.528133.
[20] Vincent P, Shareck F, Dupont C, Morosoli R, Kluepfel D. New alpha-L-arabinofuranosidase produced by *Streptomyces lividans*: cloning and DNA sequence of the abfb gene and characterization of the enzyme. Biochem J 1997;322(Pt 3):845–52. https://doi.org/10.1042/bj3220845.
[21] Wang W, Mai-Gisondi G, Stogios PJ, Kaur A, Xu X, Cui H, et al. Elucidation of the molecular basis for arabinoxylan-debranching activity of a thermostable family GH62 α-L-arabinofuranosidase from *Streptomyces thermoviolaceus*. Appl Environ Microbiol 2014;80:5317–29. https://doi.org/10.1128/aem.00685-14.
[22] Ferré H, Broberg A, Duus JØ, Thomsen KK. A novel type of arabinoxylan arabinofuranohydrolase isolated from germinated barley. Eur J Biochem 2000;267:6633–41. https://doi.org/10.1046/j.1432-1327.2000.01758.x.
[23] Koutaniemi S, Tenkanen M. Action of three GH51 and one GH54 α-arabinofuranosidases on internally and terminally located arabinofuranosyl branches. J Biotechnol 2016;229:22–30. https://doi.org/10.1016/j.jbiotec.2016.04.050.
[24] McCleary BV, McKie VA, Draga A, Rooney E, Mangan D, Larkin J. Hydrolysis of wheat flour arabinoxylan, acid-debranched wheat flour arabinoxylan and arabino-xylo-oligosaccharides by β-xylanase, α-L-arabinofuranosidase and β-xylosidase. Carbohydr Res 2015;407:79–96. https://doi.org/10.1016/j.carres.2015.01.017.
[25] Sakamoto T, Inui M, Yasui K, Hosokawa S, Ihara H. Substrate specificity and gene expression of two *Penicillium chrysogenum* α-L-arabinofuranosidases (afq1 and afs1) belonging to glycoside hydrolase families 51 and 54. Appl Microbiol Biotechnol 2012;97:1121–30. https://doi.org/10.1007/s00253-012-3978-3.
[26] Chong S-L, Battaglia E, Coutinho PM, Henrissat B, Tenkanen M, de Vries RP. The α-glucuronidase agu1 from *Schizophyllum commune* is a member of a novel glycoside hydrolase family (GH115). Appl Microbiol Biotechnol 2011;90:1323–32. https://doi.org/10.1007/s00253-011-3157-y.
[27] Rogowski A, Baslé A, Farinas CS, Solovyova A, Mortimer JC, Dupree P, et al. Evidence that GH115 α-glucuronidase activity, which is required to degrade plant biomass, is dependent on conformational flexibility. J Biol Chem 2014;289:53–64. https://doi.org/10.1074/jbc.M113.525295.
[28] Wang W, Yan R, Nocek BP, Vuong TV, Di Leo R, Xu X, et al. Biochemical and structural characterization of a five-domain GH115 α-glucuronidase from the marine bacterium *Saccharophagus degradans* 2-40t. J Biol Chem 2016;291:14120–33. https://doi.org/10.1074/jbc.M115.702944.
[29] Yan R, Vuong TV, Wang W, Master ER. Action of a GH115 α-glucuronidase from *Amphibacillus xylanus* at alkaline condition promotes release of 4-*O*-methylglucopyranosyluronic acid from glucuronoxylan and arabinoglucuronoxylan. Enzyme Microb Technol 2017;104:22–8. https://doi.org/10.1016/j.enzmictec.2017.05.004.
[30] Goldschmidt L, Cooper DR, Derewenda ZS, Eisenberg D. Toward rational protein crystallization: a web server for the design of crystallizable protein variants. Protein Sci 2007;16:1569–76. https://doi.org/10.1110/ps.072914007.
[31] Kabsch W. XDS. Acta Crystallogr D 2010;66:125–32. https://doi.org/10.1107/S0907444909047337.
[32] Winn MD, Ballard CC, Cowtan KD, Dodson EJ, Emsley P, Evans PR, et al. Overview of the ccp4 suite and current developments. Acta Crystallogr D 2011;67:235–42. https://doi.org/10.1107/S0907444910045749.
[33] Adams PD, Afonine PV, Bunkoczi G, Chen VB, Davis IW, Echols N, et al. Phenix: a comprehensive Python-based system for macromolecular structure solution. Acta Crystallogr D 2010;66:213–21. https://doi.org/10.1107/S0907444909052925.
[34] Kelley LA, Mezulis S, Yates CM, Wass MN, Sternberg MJ. The Phyre2 web portal for protein modeling, prediction and analysis. Nat Protoc 2015;10:845–58. https://doi.org/10.1038/nprot.2015.053.
[35] Emsley P, Lohkamp B, Scott WG, Cowtan K. Features and development of coot. Acta Crystallogr D 2010;66:486–501. https://doi.org/10.1107/S0907444910007493.
[36] Martinez-Abad A, Berglund J, Toriz G, Gatenholm P, Henriksson G, Lindstrom M, et al. Regular motifs in xylan modulate molecular flexibility and interactions with cellulose surfaces. Plant Physiol 2017;175:1579–92. https://doi.org/10.1104/pp.17.01184.
[37] Andrewartha KA, Phillips DR, Stone BA. Solution properties of wheat-flour arabinoxylans and enzymically modified arabinoxylans. Carbohydr Res 1979;77:191–204. https://doi.org/10.1016/s0008-6215(00)83805-7.
[38] Pitkanen L, Tuomainen P, Virkki L, Tenkanen M. Molecular characterization and solution properties of enzymatically tailored arabinoxylans. Int J Biol Macromol 2011;49:963–9. https://doi.org/10.1016/j.ijbiomac.2011.08.020.
[39] Aalbers F, Turkenburg JP, Davies GJ, Dijkhuizen L. Lammerts van Bueren, A. Structural and functional characterization of a novel family GH115 4-*O*-methyl-α-glucuronidase with specificity for decorated arabinogalactans. J Mol Biol 2015;427:3935–46. https://doi.org/10.1016/j.jmb.2015.07.006.